Universiteit Leiden
The Netherlands

The effect of replacing the axial methionine ligand with a lysine residue in cytochrome c-550 from Paracoccus versutus assessed by X-ray crystallography and unfolding: X-ray and unfolding studies of cyt c-550

Worrall, J.A.R.; Roon, A.M.M. van; Ubbink, M.; Canters, G.W.

Citation
Worrall, J. A. R., Roon, A. M. M. van, Ubbink, M., & Canters, G. W. (2005). The effect of replacing the axial methionine ligand with a lysine residue in cytochrome c-550 from Paracoccus versutus assessed by X-ray crystallography and unfolding: X-ray and unfolding studies of cyt c-550. *Febs Journal*, *272*(10), 2441-2455. doi:10.1111/j.1742-4658.2005.04664.x

Version: Publisher's Version
License: Licensed under Article 25fa Copyright Act/Law (Amendment Taverne)
Downloaded from: https://hdl.handle.net/1887/3618612

Note: To cite this publication please use the final published version (if applicable).

the FEBS Journal

The effect of replacing the axial methionine ligand with a lysine residue in cytochrome *c*-550 from *Paracoccus versutus* assessed by X-ray crystallography and unfolding

Jonathan A. R. Worrall, Anne-Marie M. van Roon, Marcellus Ubbink and Gerard W. Canters

Leiden Institute of Chemistry, Leiden University, Gorlaeus Laboratories, Leiden, the Netherlands

Keywords
axial ligand; cytochrome *c*; unfolding, peroxidase activity; X-ray crystallography

Correspondence
G. W. Canters, Leiden Institute of Chemistry, Leiden University, Gorlaeus Laboratories, PO Box9502, 2300 RA Leiden, the Netherlands
Fax: +31 71 527 4349
Tel: +31 71 527 4256
E-mail: canters@chem.leidenuniv.nl

(Received 14 January 2005, revised 9 March 2005, accepted 15 March 2005)

doi:10.1111/j.1742-4658.2005.04664.x

The structure of cytochrome *c*-550 from the nonphotosynthetic bacteria *Paraccocus versutus* has been solved by X-ray crystallography to 1.90 Å resolution, and reveals a high structural homology to other bacterial cytochromes c_2. The effect of replacing the axial heme-iron methionine ligand with a lysine residue on protein structure and unfolding has been assessed using the M100K variant. From X-ray structures at 1.95 and 1.55 Å resolution it became clear that the amino group of the lysine side chain coordinates to the heme-iron. Structural differences compared to the wild-type protein are confined to the lysine ligand loop connecting helices four and five. In the heme cavity an additional water molecule is found which participates in an H-bonding interaction with the lysine ligand. Under cryo-conditions extra electron density in the lysine ligand loop is revealed, leading to residues K97 to T101 being modeled with a double main-chain conformation. Upon unfolding, dissociation of the lysine ligand from the heme-iron is shown to be pH dependent, with NMR data consistent with the occurrence of a ligand exchange mechanism similar to that seen for the wild-type protein.

The Gram-negative, nonphotosynthetic bacterium *Paracoccus versutus* (formerly *Thiobacillus versutus* [1]) has a repertoire of respiratory chains and regulatory systems that allow it to cope with a variety of environments and different substrates as energy sources [2]. Regardless of which energy source is utilized, a class I *c*-type cytochrome, cyt *c*-550, acting as an electron-carrier is present in the respiratory chain which is homologous to the cyts c_2 found in photosynthetic bacteria [2,3]. A number of biochemical and biophysical studies on *P. versutus* cyt *c*-550 have been reported [4–14]. However, throughout these studies no 3D structure of the protein was available and a model based on the known structure of the cyt *c*-550 from *P. dentirificans* [15] was constructed to aid in interpretation of data.

All class I *c*-type cyts so far studied, undergo a dynamic equilibrium process in their ferric state which involves the dissociation of the weak methionine-S^{δ}-heme-iron bond. Such a process results in an equilibrium between low- and high-spin heme species and allows for exogenous ligands such as imidazole to bind the heme-iron [16,17]. This equilibrium also leads to cyts *c* possessing residual peroxidase activity under native conditions [18]. For exogenous ligands to gain access to the heme, sufficient movement of the loop containing the Met ligand connecting helices four and five must occur [19–22]. At present two X-ray structures of cyts c_2 exist in which the coordinating Met-iron bond is broken and the vacant heme coordination site is filled by an exogenous ligand; the imidazole adduct of *Rhodobacter sphaeroides* cyt c_2 [23] and the ammonia adduct of *Rhodopseudomonas palustris* cyt c_2 [24]. In both structures loss of Met ligation does not result in wholesale structural changes but is localized

Abbreviations
cc, cryo-cooled; cyt, cytochrome; rt, room temperature; wt, wild type.

to a few residues adjacent to the now noncoordinating Met residue.

Methionine heme-iron dissociation in ferricyts *c* is enhanced under alkaline conditions (pH ≥ 9.0) and is accompanied by a large structural rearrangement of the ligand loop [25], resulting in a Lys residue coordinating to the heme-iron [26]. For *P. versutus* ferricyt *c*-550 NMR evidence is consistent with the presence of a single alkaline species with a de-protonated amino group of a side-chain Lys replacing the native M100 [3]. This contrasts with the mitochondrial cyts *c* where a heterogenous mixture of alkaline species exists, reported to have a different coordinating Lys [26,27]. Unfolding studies on ferricyts *c* reveal that dissociation of the Met heme-iron bond is the first step on the unfolding pathway. At pH values ≥7.0 certain ligand exchange events occur during unfolding which are akin to those for the 'alkaline transition'. Moreover, it has been proposed that the structural units of cyts *c* which are responsible for the release of the Met ligand under alkaline conditions [28] are the same as those in the first step of the unfolding process [29–31].

The spectroscopic properties of a cyt *c* with a Lys residue replacing the native Met ligand were investigated with the M100K variant of *P. versutus* cyt *c*-550 [7]. This mutation resulted in a mature protein which at neutral pH and in its ferric state exhibits similar spectroscopic properties to the single species observed at alkaline pH. This amongst other evidence suggested that K100 was coordinating the heme-iron [7]. Interestingly, ligand exchange for the M100K variant at alkaline pH was not observed [7], suggesting that the 'alkaline transition' involving the dissociation of the axial ligand no longer occurs.

The present study addresses the effect on structure and unfolding upon replacing the axial Met ligand with a Lys in the M100K variant of cyt *c*-550 from *P. versutus*. We describe three X-ray structures, one of the ferric wild type (wt) and two of the ferric M100K variant. The latter confirm Lys–heme coordination. Also the effect Lys–heme coordination has on the unfolding of the M100K variant is established by way of peroxidase activity assays and NMR spectroscopy.

Results

Structure determination and overall structure of the various ferricyt *c*-550 models

For the M100K variant two X-ray datasets were collected. One at 295 K designated M100K room temperature (rt) to 1.95 Å resolution and one on a crystal at 100 K protected by a cryo-salt [32], and designated M100K cryo-cooled (cc) to 1.55 Å resolution. The structure was easily determined by molecular replacement using the structure of cyt *c*-550 from *P. denitrificans* (Protein Data Bank code: 1cot) strain LMD 22.21 [15,33]. *P. versutus* cyt *c*-550 has a high homology with the cyt *c*-550 from *P. denitrificans* with only 22 amino acids differing of which 12 are conservative changes [4]. The final models contained 121 amino acids, 32 (rt) and 138 (cc) water molecules and one heme group.

An X-ray dataset was collected for the wt protein from a single crystal at room temperature to 1.90 Å resolution. Structure determination by molecular replacement was straightforward by using the M100K(rt) structure as a search model. Crystals of the wt protein contain one monomer in the asymmetric unit with the final wt model consisting of 119 amino acids, 50 water molecules and one heme group. In all models no density was observed for the N-terminal Gln. For the wt and M100K models density up to P120 and A122, respectively, was observed. No electron-density for the 13 residues after the C-terminal helix (helix 5, residues 108–117) starting at A122 was present. This part has been reported to be highly dynamic in solution [10]. The statistics for data collection and refinement are summarized in Table 1. The program PROCHECK [34] was used to analyse conformational variations from the defined norms, with the quality of the Ramachandran plots [35] reported in Table 1. Electron density for the majority of side-chain atoms was clearly visible, although a number of surface exposed Lys residues have poor density and high thermal factors at the end of their side chain.

The polypeptide fold of ferricyt *c*-550 observed in the crystal is composed of five α-helices (residues 5–14, 57–65, 73–81, 83–90 and 108–117) and two short stretches of β-strand (21–23 and 28–30), very similar to what was reported for the ferrous form in the solution state [10]. A number of turns, consisting of two type I and four type II β-turns enable the polypeptide to wrap around the heme, Fig. 1. The average temperature factor fluctuations for the backbone atoms of the wt and M100K models are presented in Fig. 2. In all models, five regions exhibit above-average temperature fluctuations. In the wt protein these correspond to residues 23–35, 49–54, 64–65, 89–93 and 103–106 and are coloured blue in Fig. 1. For the M100K(rt) model a similar pattern of B-factors is observed although values are elevated compared to the wt and M100K (cc) model. This is most likely due to a less ordered crystal, which is also reflected in a slightly lower resolution of the data. After comparing the B-value patterns of the M100K(rt) and the wt-model, a noticeable difference

17424658, 2005, 10, Downloaded from https://febs.onlinelibrary.wiley.com/doi/10.1111/j.1742-4658.2005.04664.x by University Of Leiden, Wiley Online Library on [17/05/2023]. See the Terms and Conditions (https://onlinelibrary.wiley.com/terms-and-conditions) on Wiley Online Library for rules of use; OA articles are governed by the applicable Creative Commons License

Table 1. Data processing and refinement statistics for wt and M100K structures of ferricyt *c*-550 from *P. versutus*.

	Wild-type	M100K(rt)	M100K(cc)
Data collection and processing			
Space group	$P4_12_12$	$P2_12_12_1$	$P2_12_12_1$
Unit cell parameters (Å)			
	a = 57.1	a = 31.5	a = 30.9
	b = 57.1	b = 43.0	b = 42.9
	c = 66.6	c = 88.0	c = 87.5
No. of measured reflections	143664	56678	63104
No. of unique reflections	9898	9207	17450
R_{merge} (%)[a]	13.3 (33.3)[b]	11.8 (39.3)	3.9 (5.0)
Average I/σ(I)	20.5 (1.24)	13.6 (2.8)	20.6 (11.7)
Multiplicity	14.5 (6.6)	6.2 (5.0)	3.7 (1.9)
Completeness (%)	99.9 (97.7)	99.3 (92.5)	97.7 (82.6)
Refinement statistics			
Resolution range (Å)	43.44–1.90 (1.95–1.90)	43.85–1.95 (1.99–1.95)	43.85–1.55 (1.58–1.55)
R-factor (%)	15.8 (14.4)	18.5 (22.2)	14.7 (11.0)
R_{free}-factor (%)	19.1 (20.7)	23.3 (36.8)	20.2 (17.0)
Quality of model			
r.m.s.d bond lengths (Å)	0.013	0.009	0.012
r.m.s.d. bond angles (°)	1.16	1.16	1.44
Ramachandran plot quality			
% in most favourable region	90.9	91.0	92.0
% in additional allowed regions	9.1	9.0	8.0

[a] $R_{merge} = \Sigma_i |I_i - <I>| / \Sigma <I>$ where $<I>$ is the mean intensity of N reflections with intensities I_i and common indices h, k and l (scalepack output). [b] Values of reflections recorded in the highest resolution shell are shown in parentheses.

can be observed for residues 90–100 (Fig. 2). This suggests enhanced flexibility in the ligand-loop region upon replacing M100 with a Lys residue. For the wt structure the regions exhibiting elevated B-values show good agreement with the dynamic data obtained in solution for both oxidation states of the protein [10,11].

The heme environment of wt ferricyt *c*-550 and the M100K variant

As in all cyts *c* the CXXCH heme binding motif is present. In *P. versutus* cyt *c*-550 the side-chain thiol groups of C15 and C18 form thioether linkages with the two vinyl groups of the heme. The N-terminal α-helix (helix 1) is distorted so the thioether bond from C15 to the heme can form (Fig. 1). Such a distortion appears unique to bacterial cyts c_2 as it is not observed in the mitochondrial proteins where an additional amino acid residue in the helix is present [36]. The $N^{\varepsilon 2}$ atom of the H19 side chain provides the fifth ligand to the heme-iron with a distance to the heme-iron of 2.01 Å and a H19 $N^{\varepsilon 2}$-iron-S^{δ} M100 angle of 175°. H19 is further stabilized by a H-bond between the $N^{\delta 1}$ atom and the carbonyl oxygen of P37. In the wt structure the S^{δ} atom of M100 occupies the sixth coordination position to the heme-iron with a distance of 2.4 Å. This S^{δ} atom is also H-bonded to the hydroxyl group of Y79. This feature has been suggested to play a role in modulating the reduction potential. The length of this H-bond for *P. versutus* cyt *c*-550 is 3.8 Å. For cyt c_2 from *Rhodobacter capsulatus* a similar distance is observed, yet the reduction potential is higher by 100 mV. In cyt c_2 of *Rhodophila globiformis* this distance is 3.2 Å, yet the potential is almost 200 mV higher. Thus it would appear that a clear correlation regarding the strength of this H-bonding interaction and the modulation of the reduction potential cannot easily be made.

The heme group in the wt and M100K structures deviates from planarity and can be described as saddle shaped. Such a feature appears common to all cyts *c*, regardless of the nature of the sixth ligand to the heme-iron. In both the M100K structures clear electron density to the heme-iron is seen for the side chain of K100, confirming spectroscopic evidence that K100 is acting as a ligand to the heme-iron, Fig. 3.

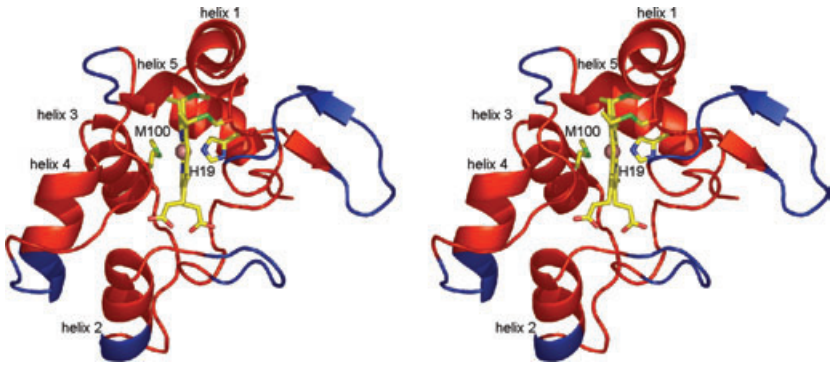

Fig. 1. Stereo view of the overall structure of wt ferricyt *c*-550 from *P. versutus* with the heme, axial ligands and the two cysteines involved in covalent linkage to the heme represented in sticks and the heme-iron shown as a sphere. The blue colouring represents regions with above average temperature fluctuations as referred to in the text. The picture was created using PYMOL Molecular Graphics System (DeLano, W.L. 2002, http://www.pymol.org).

17424658, 2005, 10, Downloaded from https://febs.onlinelibrary.wiley.com/doi/10.1111/j.1742-4658.2005.04864.x by University Of Leiden, Wiley Online Library on [17/05/2023]. See the Terms and Conditions (https://onlinelibrary.wiley.com/terms-and-conditions) on Wiley Online Library for rules of use; OA articles are governed by the applicable Creative Commons License

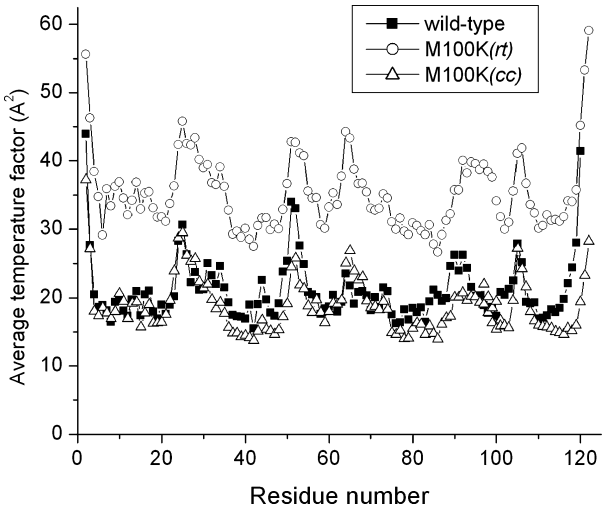

Fig. 2. Average main-chain temperature factors vs. residue number for the various structures of *P. versutus* ferricyt *c*-550.

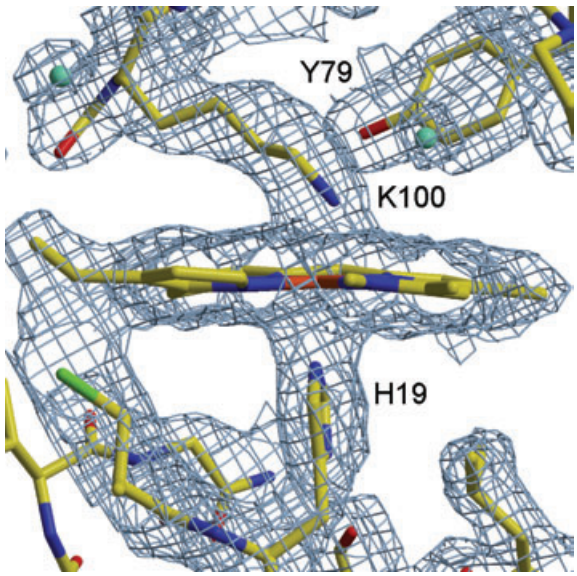

Fig. 3. $2F_o$-$2F_c$ electron density map contoured at 1.0 σ for part of the M100K(rt) structure indicating coordination of K100 to the heme-iron. The picture was created with XTALVIEW [59].

The bond lengths for the coordinating N^{ζ} and N^{ε} atoms of K100 and H19 are 1.92 and 1.96 Å, respectively. For both coordinating atoms, the distance to the heme-iron is shorter than in the wt structure along with a decreased H19 N^{ε}-iron-N^{ζ} K100 angle of 171°. Despite the shorter axial ligand distances the iron-pyrole nitrogen angles (175°) in the porphyrin ring remain approximately the same as in the wt structure (177°).

The heme environment is further characterized by an extensive network of H-bonds involving buried water molecules, the heme propionate groups and side- and main-chain atoms of nearby residues (Fig. 4, Table 2). A noticeable difference in the heme cavity between the wt and both M100K structures is the presence in the latter of an additional water molecule adjacent to K100 (Fig. 4B). This water, wat6, is within H-bonding distance to the coordinating K100 N^{ζ} atom and also to wat3 (Table 2). Wat3 makes further H–bonding interactions with the carbonyl groups of V80 and F102 as noted also in the wt structure. The presence of wat6 therefore results in the formation of a buried two-water chain connecting the K100 ligand to two different backbone substructures of the protein (helix 3, V80 and the ligand loop, F102; Fig. 4B).

Structural differences between wt ferricyt *c*-550 and the M100K(rt) variant

The overall polypeptide fold of the wt protein is maintained for the M100K variant, with an r.m.s.d. for the backbone atoms of 0.4 Å. Significant deviations for main- and side-chain atoms in the ligand loop containing the K100 are however, observed. To accommodate K100 as a ligand a number of main-chain atoms are displaced relative to their positions in the wt structure. Although backbone deviations are detected at the start of the ligand loop, the largest changes are observed in the region between the amide nitrogen of K100 and the amide nitrogen of L104 (Fig. 4C). This movement results in a positional change of a surface water molecule (wat12). Wat12, found also in the wt structure, makes H-bonds to the backbone amides of T101 and F102. In the M100K structure wat12 moves 1.24 Å relative to its position in the wt structure and therefore maintains its H-bonding interactions with this region of the ligand loop (Fig. 4C).

For a number of Lys residues complete electron density for the side chain was not observed. Nevertheless, for K97 density is observed up to the Cγ atom in wt and both M100K structures, allowing for good positional visualization of the side chain. From this density it is clear that the side-chain orientation of K97 in the two structures is different. In the wt structure the side chain slithers along the side of the protein surface, whereas in the M100K structure it points out into the solvent (Fig. 4C). The position of the K99 side chain is also different. In the wt structure a H-bonding interaction is made with the carbonyl oxygen of K54 (2.8 Å). Final refinement of the M100K(rt) structure positions the K99 side chain in such a way so as to increase this H-bonding distance to 3.1 Å. The

17424658, 2005, 10, Downloaded from https://febs.onlinelibrary.wiley.com/doi/10.1111/j.1742-4658.2005.04664.x by University Of Leiden, Wiley Online Library on [17/05/2023]. See the Terms and Conditions (https://onlinelibrary.wiley.com/terms-and-conditions) on Wiley Online Library for rules of use; OA articles are governed by the applicable Creative Commons License

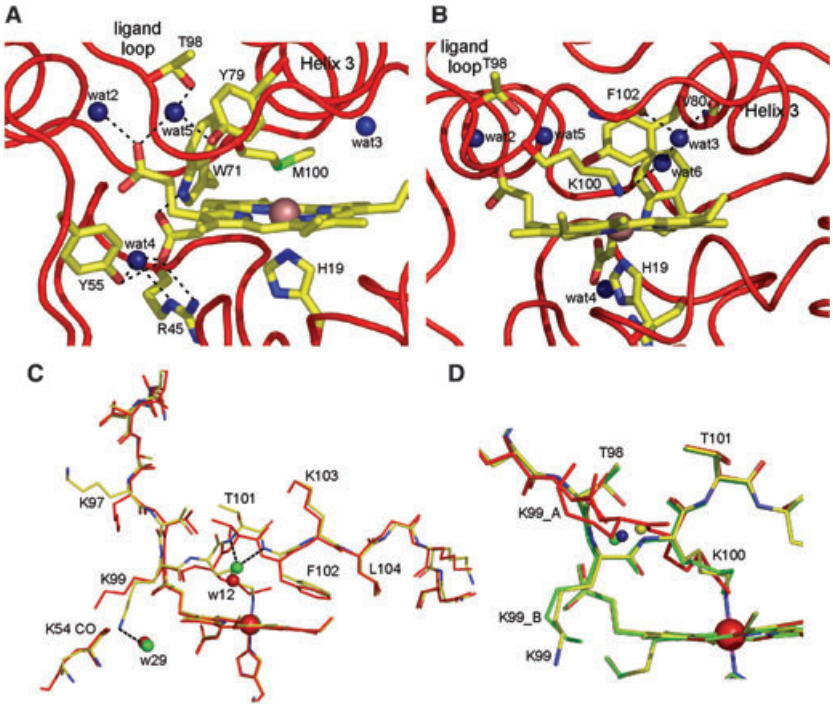

Fig. 4. Close up of the heme binding pocket of (A) wt and (B) the M100K(rt) variant of ferricyt *c*-550, with the positions of the buried water molecules found around the heme cavity depicted as blue spheres. H–bonding interactions are indicated with dashed lines and can be further referred to in Table 2. (C) Overlay of part of the axial ligand loop (residues 92–107) for the wt (red) and M100K(rt) (yellow) structures of cyt *c*-550. Two surface water molecules in each structure are indicated as spheres [red wt; green M100K(rt)] with the H-bonding interactions indicated for the M100K structure (w12:backbone amides of T101 and F102, w29:N^{ζ} of K99). (D) Overlay of part of the K100 ligand binding loop for M100K(rt) and (cc) structures showing the double conformation modeled in the latter. In yellow is the (rt) structure, with red and green conformer A and B of the (cc) structure, respectively. The position of wat5 which H-bonds to the side chain of T98 is indicated [blue (rt) structure; yellow, conformer A; green, conformer (B)].

different orientation of the K99 side chain now allows for an H-bonding interaction to a surface water molecule (wat29) with a distance of 2.9 Å (Fig. 4C). This water is also present in the wt structure and raises the possibility that the K99 side chain in both proteins can adopt two conformations stabilized by H-bond interactions. Finally, a change in the side-chain orientation of F102 is observed. In the wt model the ring is planar with respect to the heme, whereas in the M100K structure it is rotated away (Fig. 4C).

Dynamics in the K100 ligand loop detected at cryo-temperatures

The trapping of different conformations in protein segments which are dynamic in solution can be visualized by X-ray crystallography [37]. This is illustrated for the M100K variant from a dataset measured at 100 K. Following a number of refinement cycles, positive difference density was clearly visible in the vicinity of K99. The final results of model building and refinement led to a model with residues 97–101 situated in the Lys-ligand loop having a double main-chain conformation (assigned A and B; Fig. 4D). Refinement of each conformer with half occupancy resulted in the lowest R_{free}. Although no complete side-chain density is observed for K99 it is still possible to visualize its orientation in both conformers. For the M100K(rt) structure, above average B-factors compared with the wt model were seen in this region, indicating increased mobility (Fig. 2). Also the pattern of B-factors in this region for the M100K(cc) model is no longer above average which is most likely due to the modeling of two conformations [37] (Fig. 2). Data at 100 K for a cryo-cooled wt crystal protected in the same cryo-salt, resulted in no extra electron density in this region (data to 1.8 Å resolution, not shown). It would therefore appear that the coordination of K100 to the heme-iron has an effect on the dynamics in this region of the protein, which at cryo-temperatures leads to the visualization of two conformers.

On comparing the main-chain torsion angles and coordinates of the two conformers it is apparent that conformer B has almost identical geometry and coordi-

17424658, 2005, 10, Downloaded from https://febs.onlinelibrary.wiley.com/doi/10.1111/j.1742-4658.2005.04664.x by University Of Leiden, Wiley Online Library on [17/05/2023]. See the Terms and Conditions (https://onlinelibrary.wiley.com/terms-and-conditions) on Wiley Online Library for rules of use; OA articles are governed by the applicable Creative Commons License

Table 2. Hydrogen bonding interactions involving buried water molecules (w) and the carboxylates of the heme propionates (6 and 7) found in the heme cavity of wt and M100K(rt) structures of *P. versutus* ferricyt *c*-550.

wt	Donor/acceptor	Å	M100K	Donor/acceptor	Å
w4	N Ser49	3.2	w4	N Ser49	3.2
	N^{ε} Arg45	2.8		N^{ε} Arg45	2.8
	CO Lys46	2.7		CO Lys46	2.7
	N Ala48	3.3		N Ala48	3.2
	OH Tyr55	3.8		OH Tyr55	3.7
w2	N Ile59	2.9	w2	N Ile59	2.9
	N Gly58	3.3		N Gly58	3.4
	CO Lys97	2.7		CO Lys97	2.7
w5	OH Tyr79	2.8	w5	OH Tyr79	2.7
	$O^{\gamma 1}$ Thr98	2.8		$O^{\gamma 1}$ Thr98	2.9
w3	CO Phe102	3.0	w3	CO Phe102	2.7
	CO Val80	2.8		CO Val80	2.7
			w6	N^{ε} Lys100	2.8
				w3	2.9
7-O1A	w4	2.8	7-O1A	w4	2.7
	OH Tyr55	2.6		OH Tyr55	2.6
	NH_2 Arg45	3.0		NH_2 Arg45	2.9
7-O2A	w4	3.2	7-O2A	w4	3.2
	$N^{\varepsilon 1}$ Trp71	2.9		$N^{\varepsilon 1}$ Trp71	2.9
	N Ala48	3.2		N Ala48	3.0
6-O1D	N Gly56	2.8	6-O1D	N Gly56	2.8
6-O2D	w2	2.7	6-O2D	w2	2.7
	w5	2.9		w5	2.9
	N K99	3.0		N K99	3.0

nates as the M100K model determined at room temperature (Table 3, Fig. 4D). Conformer A, on the other hand, has an r.m.s.d. of 1.4 Å for the main-chain atoms of residues 97–101 relative to the wt structure and exhibits significant geometry changes particularly for T98 and K99 (Table 3). Furthermore, the side-chain position of K99 is different, with the final refinement positioning it in such a way so as to no longer cover part of the heme (Fig. 4D). From solvent accessibility calculations using the program NACCESS v2.1.1 (http://wolf.bms.umist.ac.uk/naccess) the position of the K99 side chain in conformer A results in the heme having an increased accessible surface area (ASA): 148 $Å^2$ compared to 64 and 68 $Å^2$ for the wt and the M100K(rt) structures, respectively. A further change as a result of trapping conformer A is observed for a buried water molecule, wat5 which moves 1.6 Å relative to its position in conformer B so as to maintain its H-bonding interactions (Fig. 4D).

Effect of the M100K mutation on the stability of the native state

The effect on protein stability upon introduction of a Lys ligand to the heme-iron has been assessed for the M100K variant. At pH 4.5 the UV/Vis spectrum of the ferric M100K variant displays a number of differences compared to wt [7], the most prominent being the absence of the 695-nm band, indicative of Met-S^{δ}-iron coordination. Upon titrating increasing amounts of guanidinium hydrochloride (GdmHCl) the protein unfolds resulting in the perturbation of a number of electronic absorption bands and the appearance in the spectrum of new ones. One of these, a band at 623 nm, grows into the spectrum indicating a change from low- to high-spin heme. In analogy to a previous study with the wt protein [11], we ascribe this to loss of the sixth ligand to the heme. Therefore, K100 like M100 dissociates from the heme as the protein unfolds. However, it is apparent from Fig. 5A and from the equilibrium unfolding parameters (midpoint concentrations, C_m, slopes, m, and the derived free energy in the absence of denaturant, ΔG_{unf}, see Experimental procedures; Table 4) that substitution of the M100 ligand for a Lys results in a significant change in the thermodynamic stability, with a decrease in C_m corresponding to a 3.1 kcal·mol^{-1} decrease in ΔG_{unf} compared to the wt protein.

Peroxidase activity of the M100K variant

In the native state ferricyt *c*-550 is able to catalyse H_2O_2 reduction with concomitant oxidation of a reducing substrate albeit with an extremely low rate [18]. Unfolding by addition of chemical denaturants [12,13]

Table 3. Main-chain torsion angles for part of the ligand loop of wt ferricyt *c*-550, the M100K(rt) structure and the two conformers, A and B, of the M100K(cc) structure.

	Wild-type	M100K(rt)	M100K(cc) conformer (A)	M100K(cc) conformer (B)
Residue	φ/ψ	φ/ψ	φ/ψ	φ/ψ
K97	−76.9/133.2	−88.1/137.6	−99.8/125.7	−90.5/138.5
T98	−117.5/134.7	−133.0/144.5	−162.8/146.9	−129.7/142.8
K99	−90.4/−7.5	−89.0/9.8	−104.4/0.72	−87.6/2.3
M/K100	−117.8/120.9	−163.7/145.3	−94.5/100.67	−160.5/154.9
T101	−117.5/−3.3	−124.9/0.48	−119.8/−2.7	−129.9/−9.1

17424658, 2005, 10, Downloaded from https://febs.onlinelibrary.wiley.com/doi/10.1111/j.1742-4658.2005.04664.x by University Of Leiden, Wiley Online Library on [17/05/2023]. See the Terms and Conditions (https://onlinelibrary.wiley.com/terms-and-conditions) on Wiley Online Library for rules of use; OA articles are governed by the applicable Creative Commons License

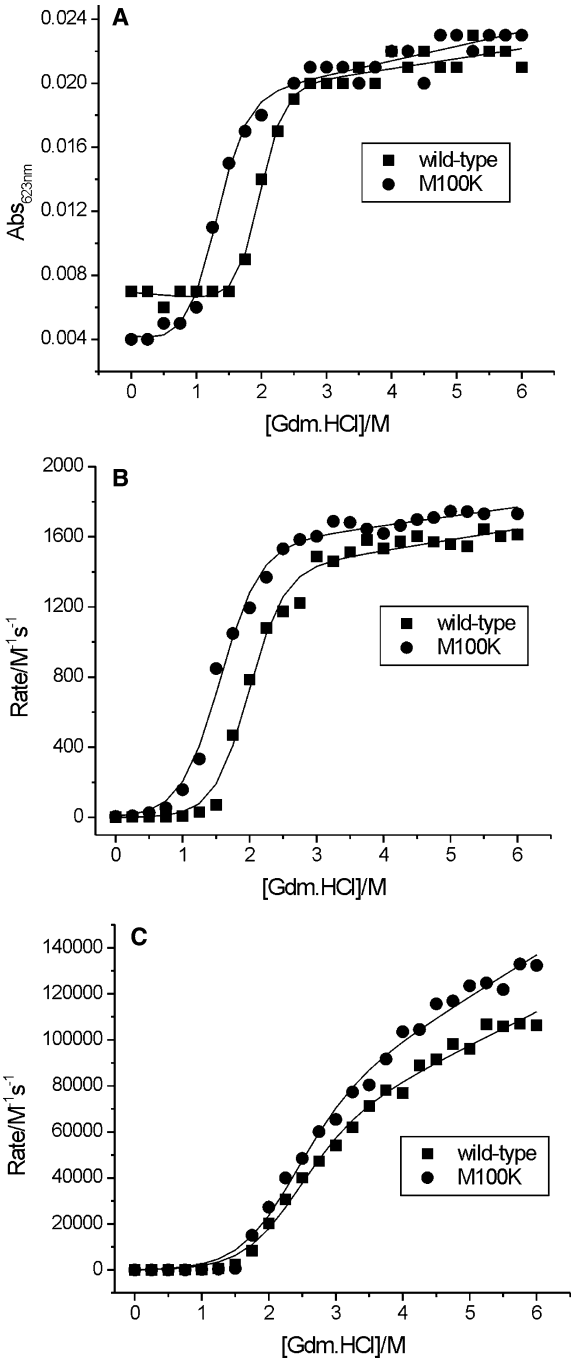

Fig. 5. Equilibrium unfolding parameters at 298 K plotted as a function of [GdmHCl] for the M100K ferricyt *c*-550. (A) Intensity change of the electronic absorption band at 623 nm at pH 4.5. (B) The peroxidase activity, pH 4.5 and (C) peroxidase activity at pH 7.0. Data for the ferric *wt* protein is included for comparison, and all data are fitted to a two-state equilibrium unfolding model.

or detergents [14] enhances the rate due to the release of the sixth axial ligand from the heme-iron which allows for the peroxide anion to bind. At pH 4.5 the mid-point of the unfolding transition (C_m) for the M100K variant monitored by peroxidase activity is again considerably shifted compared to that of the wt protein (Fig. 5B). Furthermore, in the absence of denaturant the second-order rate constant for peroxidase activity is some three times higher for the M100K variant than for the wt protein (6.1 ± 0.1 vs. 2.1 ± 0.3 $M^{-1}\cdot s^{-1}$). These results imply that Lys heme-iron coordination is weaker than Met heme-iron coordination at pH 4.5 in cyt *c*-550. Moreover, the observation of peroxidase activity in the absence of denaturant for the M100K variant provides further evidence that the equilibrium process involving the sixth ligand dissociating from the heme-iron is not exclusive to Met coordination.

At pH 7.0 despite the unfolding curves being very similar (Fig. 5C), the activity at zero denaturant is some 20 times lower for the M100K variant (~ 0.1 $M^{-1}\cdot s^{-1}$) than for the wt protein. This implies that peroxidase activity is now much more inhibited by the presence of the coordinating amino group of the Lys at pH 7.0, i.e. there is less of the five-coordinate peroxidase active species present due to a stronger ligand interaction with the heme-iron suppressing the bond-breaking equilibrium.

Unfolding of the M100K variant monitored by ^{1}H NMR at pH 7.0

At pH 7.0 the unfolding of ferricyts *c* involves coupling between structural transitions and heme-ligand exchange events [30]. The latter occur as a direct result of the dynamic equilibrium involving dissociation of the axial Met ligand. This results in deprotonated protein based ligands such as Lys, His and if available the N-terminal α-amino group competing for the vacant coordination site [11,31,38–40]. Owing to the paramagnetic properties of a low-spin ferriheme, misligated heme species can be readily identified by ^{1}H NMR. Hyperfine shifted resonances belonging to protons of heme substituents are extremely sensitive to the chemical nature of the axial ligands to the heme-iron [41]. Upon replacing the native Met ligand with either an exogenous or protein-based ligand a change in the distribution of the unpaired electron-spin density on the heme occurs resulting in changes in the chemical shifts and T_1 relaxation times of the hyperfine shifted signals [42]. This is illustrated by the comparison of the ^{1}H spectrum of wt ferricyt *c*-550 with that of the M100K variant (Fig. 6) and from the proton T_1 relaxation times derived from the heme-methyl peaks (180 vs. 95 ms for the M100K and wt proteins, respectively).

17424658, 2005, 10, Downloaded from https://febs.onlinelibrary.wiley.com/doi/10.1111/j.1742-4658.2005.04664.x by University Of Leiden, Wiley Online Library on [17/05/2023]. See the Terms and Conditions (https://onlinelibrary.wiley.com/terms-and-conditions) on Wiley Online Library for rules of use; OA articles are governed by the applicable Creative Commons License

Table 4. Thermodynamic parameters (298 K) for the equilibrium unfolding of wt ferricyt *c*-550 and the M100K variant in the presence of GdmHCl monitored by the intensity change of the electronic absorbance band at 623 nm, and the peroxidase activity. ΔG_{unf} units are kcal·mol^{-1}, *m* are kcal·mol^{-1}·M^{-1} and C_m are M.

		Abs_{623nm}			Peroxidase assays		
Protein	pH	ΔG_{unf}	*m*	C_m	ΔG_{unf}	*m*	C_m
wt	4.5	6.4 ± 1.6	3.2 ± 0.8	2.0 ± 1.0	4.5 ± 0.5	2.3 ± 0.3	2.0 ± 0.5
	7.0				3.2 ± 0.4	1.4 ± 0.2	1.6 ± 0.6
M100K	4.5	3.3 ± 0.9	2.5 ± 0.6	1.3 ± 0.7	3.1 ± 0.3	2.0 ± 0.2	1.6 ± 0.3
	7.0				3.0 ± 0.4	1.4 ± 0.2	2.0 ± 0.6

Upon addition of GdmHCl the changes in the spectrum of the M100K variant are reminiscent of those observed previously with wt cyt *c*-550 [11]. The native heme-methyl signals decrease in intensity and are replaced by peaks of lower intensity arising from partially unfolded low-spin forms of the protein. At low [GdmHCl] native and partially unfolded protein species are visible. This indicates that these forms are in slow-exchange with one another on the NMR timescale with a $k_{ex} < 6000\ s^{-1}$, estimated from the relationship $k_{ex} = 2\pi\Delta\delta/\sqrt{2}$. The new low-spin peaks were identified as arising from heme-methyl signals by measuring the proton T_1 relaxation times as described previously for the wt and two site-directed variants, K99E and H118Q [11]. The peaks labelled A_1/A_2 in Fig. 6B have T_1 times of 146 ms falling into the range for heme-methyl protons with Lys/His heme-iron coordination. For signals B_1/B_2 T_1 times were lower and are in the region of 57 ms. These were assigned to heme-methyl protons belonging to a species with His/His coordinated heme. Therefore a mixture of non-native Lys/His, His/His and 'native' Lys/His heme coordination is present at low [GdmHCl]. These results indicate that dissociation of the K100 occurs in a similar manner as for M100 coordination and that unlike at alkaline pH, unfolding using GdmHCl induces a ligand-exchange mechanism.

Discussion

Bacterial cytochromes c_2 show a greater diversity in amino acid homology, size and reduction potentials compared to their mitochondrial counterparts. As part of the present work the structure of cyt *c*-550 from *P. versutus* has been determined by X-ray crystallography, allowing for a comparison in terms of overall structure and heme environment to be made with other members of the class I monoheme cyt *c* family. In addition, the effect on structural and unfolding properties of replacing the axial methionine ligand with a lysine residue has been further assessed.

Cyt *c*-550 from *P. versutus* exhibits high a structural homology with the cyts c_2 from *P. denitrificans* [15], *R. capsulatus* [43], and *R. sphaeriodes* [23] (Fig. 7) with *R. capsulatus* a high-potential cyt c_2. Cyt *c*-550, on the other hand, is a low-potential cyt c_2 with a reduction potential of +250 mV vs. NHE, pH 7.0 [3]. The recent structures of a high-potential cyt c_2 (E = +350–450 mV vs. NHE) in both oxidation states have given insight into a possible explanation for their elevated reduction potentials [24,44], assigned to a lack of movement of a highly conserved water molecule upon oxidation of the heme to the Fe^{3+} state. This water is present as wat5 in the cyt *c*-550 structure (Fig. 4A). For mitochondrial and low-potential bacterial cyts, this water moves closer to the heme-iron upon oxidation which along with the subsequent alteration of the surrounding H-bonding network serves to stabilize the positive charge on the heme due to the negative end of the water dipole pointing towards it [45]. The H-bonding rearrangement abolishes the interaction of wat5 with the $N^{\delta 2}$ of N52 (yeast cyt *c* numbering). Such an interaction is not present in cyt *c*-550 due to residue 59 (residue 52 in yeast) being an Ile. Interestingly, mutagenesis of N52 in yeast iso-1-cyt *c* to an Ile results in the loss of wat5 and a resulting decrease in reduction potential attributed to the elimination of a repulsive interaction between the N52 dipole and the positively charged heme group [46]. On average the distance of wat5 from the heme-iron in the ferrous form for the mitochondrial and low-potential proteins is ≈ 6.6 Å, decreasing to ≈ 5.0 Å in the ferric form. In high-potential cyts c_2 the average distance in either oxidation state is ≈ 6.8 Å. In *P. versutus* ferricyt *c*-550 wat5 has a distance to the heme-iron of 7.5 Å, considerably longer than the above and suggesting a weaker interaction with the positive charge on the heme-iron. It could be speculated that wat3, adjacent to the M100 ligand at a distance of 6.0 Å to the heme-iron helps to compensate for the somewhat longer distance of wat5. Wat3 is present also in *P. denitrificans* cyt *c*-550, but is absent in all other cyt c_2 species and mitochondrial

17424658, 2005, 10, Downloaded from https://febs.onlinelibrary.wiley.com/doi/10.1111/j.1742-4658.2005.04664.x by University Of Leiden, Wiley Online Library on [17/05/2023]. See the Terms and Conditions (https://onlinelibrary.wiley.com/terms-and-conditions) on Wiley Online Library for rules of use; OA articles are governed by the applicable Creative Commons License

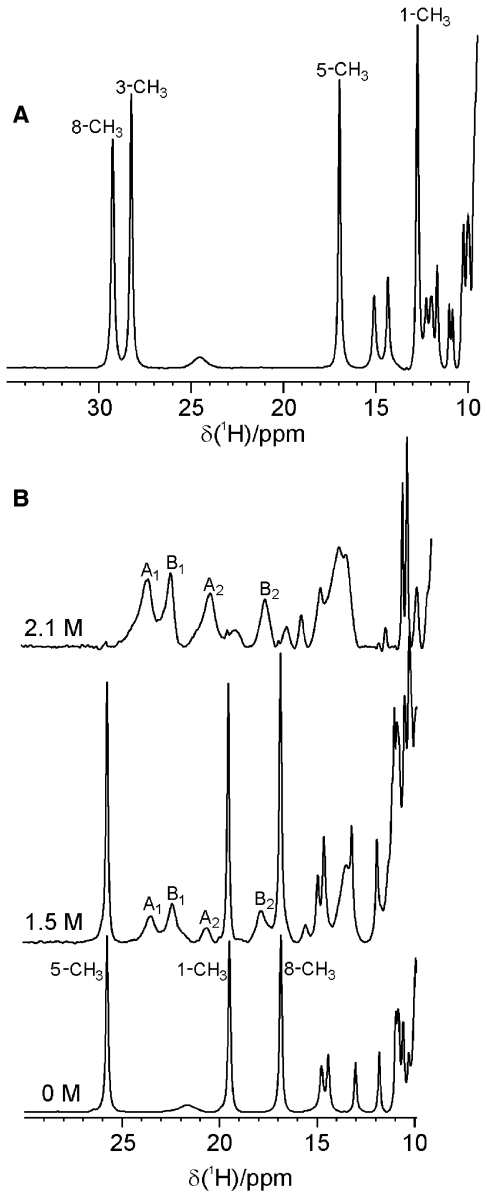

Fig. 6. Down-field region of the ^{1}H NMR spectra at 600 MHz, 298 K, pH 7.0 of (A) wt ferricyt *c*-550 in the absence of GdmHCl and (B) the ferric M100K variant in the presence of increasing amounts of GdmHCl. In A the signals arising from the four hyperfine shifted heme-methyl groups are labeled accordingly. For the M100K variant, peaks corresponding to three hyperfine shifted heme-methyl substituents are labeled, with the fourth, heme-methyl 3, found in the diamagnetic region of the spectrum [9]. The signals labeled A_1/A_2 and B_1/B_2 arise from non-native heme ligation as the protein unfolds.

cyts *c* for which structures are reported. Furthermore, the H-bonding pattern of wat5 has a higher similarity to the cyt c_2 from *R. capsulatus* than to other bacterial or mitochondrial proteins due to the absence of the

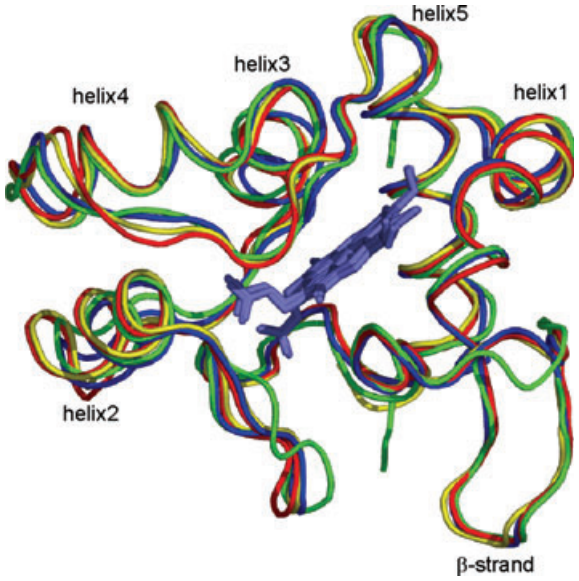

Fig. 7. Overlay of the main-chains of three bacterial *c*-type cytochromes with the highest structural homology to *P. versutus* cyt *c*-550. Yellow *P. denitrificans* cyt *c*-550 (1cot, 1.7 Å [15]), blue *R. capsulatus* cyt c_2 (1c2r, 2.5 Å [43]), green *R. sphaeriodes* cyt c_2 (1cxc, 1.6 Å [23]) and red *P. versutus* cyt *c*-550 (2bgv, 1.90 Å).

above mentioned Asn residue. The fact that *R. capsulatus* cyt c_2 is high-potential and lacks both the Asn and wat3, further suggests a role for wat3 in *P. versutus* and *P. denitrificans* in stabilizing the oxidized form.

To assess the effect on the ligand loop in *c*-type cyts upon replacing the Met ligand with another protein based ligand, the structure of the M100K variant was determined. The refined M100K structure confirmed previous spectroscopic evidence that the Lys side chain is buried in the protein interior with the amino group coordinating to the ferric heme-iron [7]. The K100 N^{ζ}-iron distance of 1.9 Å is considerably shorter than the Fe-N distance in Fe-NH_3 model complexes (2.1 Å) and in the cyt c_2 ammonia adduct (2.1 Å) [24]. Furthermore, the distance is longer for Lys heme-iron coordination in the octaheme tetrathionate reductase from *Shewanella oneidensis* MR-1, 2.2 Å [47], and also for the N-terminal amino coordination in cytochromes *f*, 2.1 Å [48]. The distance is closer to the Fe-O distance in Fe-OH complexes and five coordinate hydroxo-iron(III) porphyrins (≈ 1.9 Å) [49,50].

Structural changes in the loop connecting helices 4 and 5 are observed upon accommodating a Lys ligand. These involve both side- and main-chain atoms with residues which exhibit the largest changes located either side of the K100 ligand (Fig. 4C). The changes in this region are not as large as those observed in the imidazole or ammonia cyt c_2 adducts [23,24] which

17424658, 2005, 10, Downloaded from https://febs.onlinelibrary.wiley.com/doi/10.1111/j.1742-4658.2005.04664.x by University Of Leiden, Wiley Online Library on [17/05/2023]. See the Terms and Conditions (https://onlinelibrary.wiley.com/terms-and-conditions) on Wiley Online Library for rules of use; OA articles are governed by the applicable Creative Commons License

show peptide bond flipping and 180° rotation of side chains. This is most likely due to the fact that in the latter the absence of coordination by the Met does not impose any conformational constraints and the localized region of the loop affected by release of the Met ligand is then free to adopt a new low energy conformation. For the M100K(cc) structure residues 98–100 in conformer A display quite large deviations and geometry changes (Table 3, Fig. 4D). Interestingly, these residues have been singled out in *R. capsulatus* cyt c_2 to be involved in 'hinge' dynamics [19]. This study indicated that the dynamic equilibrium of Met-S^{δ}-iron bond breaking, allowing access to the heme-iron of exogenous ligands, involves residues 93–100 (97–104 in *P. versutus*). In particular residues 93 and 95 of *R. capsulatus* cyt c_2 have a profound effect on the kinetics of the rearrangement of the 'open' and 'closed' forms of the ligand loop [19]. Therefore, conformer A may be considered as the open form, albeit with the axial ligand still intact, with the main- and side-chain atoms of K99 flipped up and away from the heme resulting in an increased solvent exposure of the heme.

The presence of an additional water molecule, wat6, in the heme cavity for the M100K variant is a new feature in this region of the structure compared to wt (Fig. 4A,B). Whether this water molecule, which makes H-bonding interactions with the N^{ζ} atom of K100 and wat3, influences any physical property of the variant is open to speculation. The reduction potential of the M100K variant is −77 mV vs. the NHE, which lies between *bis*-histidine coordinated cyt *c* (+41 mV vs. SHE [51]) and the alkaline form with Lys-His coordination (−205 mV vs. SHE [52]). An increased solvent exposure of the heme has been shown to contribute significantly to lowering the reduction potential of the latter form [25,52,53], and it was noted that conformer A of the M100K variant displayed a substantially increased heme ASA. The lower reduction potential compared to the *bis*-His cyt *c* is probably a reflection of the more basic ζ-amino group of the coordinating K100, with the H-bonded water molecule found in the X-ray structure increasing the electron donating power of the coordinating amino group which in turn can decrease the reduction potential more than may be expected for this type of ligand interaction.

Substitution of the axial Met ligand with a Lys influences ligand dissociation and protein stability. The latter point is illustrated at acidic pH where a decreased unfolding mid-point compared to wt is observed (Fig. 5). This indicates a weaker Lys–N^{ζ}–iron interaction which is also inferred from the enhanced peroxidase activity in the absence of denaturant. At pH 7.0, the mid-point of the unfolding transition for the M100K variant and wt are almost identical yet the rate in the absence of denaturant is some 20-times lower for the variant. This indicates a stronger ligand interaction leading to a lower percentage of high-spin peroxidase active species. As unfolding monitored through peroxidase activity can be interpreted as a measure of localized unfolding of the axial ligand loop, i.e. the lowest free-energy intermediate [12], the observation that both proteins display similar unfolding curves at pH 7.0, yet have different ligand strengths, may indicate that the local unfolding of this region is not under sole control of the axial ligand. If so then this suggests the region around the K100 ligand is less stable than in the wt protein. This is also inferred from the structural data, where despite structural changes being minimal the trapping of two main-chain conformations and increased B-factors at 295 K suggests that the presence of the coordinating Lys in some way can influence the dynamics of the ligand loop.

Hoang *et al.* [28] have demonstrated that the same structural units which govern the early cooperative unfolding events of horse heart cyt *c* are also involved in triggering the conformational change resulting in ligand-exchange at alkaline conditions. Despite this, no conformational ligand switching is observed at alkaline pH for the M100K variant. This contrasts with the unfolding data accumulated in this study which show that the early unfolding of the M100K variant involves the breaking of the Lys-N^{ζ}-iron bond coupled with the dynamic process of ligand exchange. It thus seems likely that the mechanism of release of the axial ligand under alkaline conditions and in the presence of GdmHCl is different. Under alkaline conditions release of the axial ligand is postulated to arise from the deprotonation of an ionizable group (the 'trigger') the nature of which is as yet unknown. For the M100K variant it seems likely that the deprotonation of the trigger is simply not enough to initiate release of the strong Lys-N^{ζ}-iron bond. In the case of unfolding with GdmHCl, it may be that the disruption of electrostatic interactions due to its ionic nature is enough to trigger the release of the Lys ligand.

In summary, the structure of ferric wt cyt *c*-550 from *P. versutus* shows a high structural homology with both low- and high-potential bacterial *c*-type cyts of similar size with a possible role for a nonconserved water (wat3) in stabilizing the cationic ferriheme proposed. The structure of the M100K variant clearly indicates that the lysine coordinates the heme-iron, with slight structural changes in the ligand loop brought about so as to accommodate the longer side

17424658, 2005, 10, Downloaded from https://febs.onlinelibrary.wiley.com/doi/10.1111/j.1742-4658.2005.04864.x by University Of Leiden, Wiley Online Library on [17/05/2023]. See the Terms and Conditions (https://onlinelibrary.wiley.com/terms-and-conditions) on Wiley Online Library for rules of use; OA articles are governed by the applicable Creative Commons License

chain. This appears also to translate into increased dynamics in the ligand loop, which under cryo-cooled conditions results in the trapping of two main-chain conformations. A further difference found in the M100K structures compared to the wt is the presence of wat6 in the heme cavity. This water H-bonds to the K100 ligand most likely increasing the basicity of the N-donor to the heme-iron and lowering the reduction potential further than may be expected for such an interaction. Finally, from peroxidase activity assays in the absence of denaturant the dynamic equilibrium of Met ligand dissociation observed in all *c*-type cyts occurs also with Lys-heme-iron coordination. Nevertheless this does not result in a ligand-exchange mechanism at alkaline pH for the M100K variant which contrasts to what occurs in the presence of the chemical denaturant GdmHCl as ascertained in this study by NMR.

Experimental procedures

Expression and purification of *P. versutus* cyt c-550 and the M100K variant

Wild-type cyt *c*-550 was heterologously expressed in *P. denitrificans* strain 2131 containing the pEG400.Tv1 plasmid [18]. The M100K variant was constructed as previously reported [7] and expressed in *Escherichia coli*. Purification of both proteins was carried out as reported [18]. Purity of samples for crystallization experiments and unfolding studies was checked by SDS/PAGE and from absorbance ratios in the UV-vis spectrum; $A_{525}/A_{280} \geq 0.4$ for ferric wt protein and $A_{526}/A_{280} \geq 0.4$ for the ferric M100K variant.

Crystallization trials and X-ray data collection

Prior to crystallization trials protein solutions were oxidized with a 1 mM solution of $K_3[Fe(CN)_6]$. Samples were then concentrated and exchanged into water (MilliQ) by ultra-filtration methods (Amicon), followed by filtering through a low-protein binding filter (0.22 μm; Millipore) to remove dust particles and protein aggregates. Protein concentrations were determined spectrophotometrically from the absorbance at 409 nm ($\varepsilon = 132\ mM^{-1}$) for wt [3] and 406 nm ($\varepsilon = 187\ mM^{-1}$) for the M100K variant [7]. Final protein concentrations ranged between 5 and 8 $mg{\cdot}mL^{-1}$. Crystallization experiments for the wt and M100K variant of ferricyt *c*-550 were carried out using the sitting drop vapour diffusion method at 295 K using equal volumes of protein and reservoir solutions. Dark red crystals of the M100K variant suitable for X-ray crystallography were grown within 24–48 h, from 1 μL of protein solution mixed with 1 μL of reservoir solution containing 0.1 M bicine pH 9.0 and 3.2 M ammonium sulfate. For the wt protein obtaining suitable crystals was more difficult. Crystalline networks of protein were constantly observed in the drops and these were repeatedly dissolved by addition of 1 μL of water. Attempts to slow down the crystallization process with 8.7% glycerol in the reservoir solutions [54] were to no avail. After 2–3 weeks and repeated dissolving of the crystalline networks a single dark red crystal suitable for X-ray diffraction was obtained grown from 0.1 M bicine pH 9.0 and 3.2 M ammonium sulfate.

X-ray diffraction data of the wt and M100K crystals were collected on an in-house beam using a MAR345 Image Plate detector. The crystals were mounted in a capillary and datasets at 295 K and were measured to 1.90 and 1.95 Å resolution for the wt and M100K proteins, respectively. For cryo-cooled M100K crystals, data was obtained at the European Synchotron Radiation Facility at beamline BM30a using a MARCCD detector. A suitable cryo-protectant was found consisting of a 20 : 10 (v/v) lithium sulfate:ammonium sulfate solution. The crystals were mounted in cryo-loops (Hamilton) and passed quickly through the cryo-protectant solution, followed by flash-freezing in a nitrogen gas stream at 100 K. A dataset was collected to 1.55-Å resolution. All collected data were indexed, integrated and scaled with HKL2000 [55].

Structure determination and refinement

The structure of the M100K(rt) was solved by molecular replacement using the program MOLREP [56] from the CCP4 program suite [57] using the ferricyt *c*-550 structure from *P. denitrificans* (PDB code 1cot [15]) as the search model. A solution was obtained with an R-factor of 36.3% and a correlation coefficient of 65.9. After several rounds of rigid body and restrained refinement with REFMAC5 [58], the correct amino acids were built in manually using XTALVIEW [59], followed by automatic solvent building using ARP/WARP [60]. Final restrained refinement resulted in a model having an R-factor of 17.5% (R_{free} 23.1%). This refined model was used for further refinement using the high resolution data of the M100K obtained at 100 K, keeping the same R_{free} set as the M100K(rt). Upon inspection of a F_o-F_c difference density map, a double conformation of the main chain running from residue K97 to T101 could be modeled and refined. After final refinement of the model, including refinement of anisotropic B-factors, a model was obtained having an R_{free} of 20%. The unrealistic value of the $I/\sigma(I)$ for the highest resolution shell is because the crystal would apparently diffract to a much higher resolution but due to technical difficulties at the beamline the collection of higher resolution data was not possible. The structure of wt ferricyt *c*-550 was solved by molecular replacement using the M100K(rt) structure as the search model (*R*-factor 39.3% and correlation coefficient 62.7). Refinement and solvent building was carried out as described for the M100K(rt) with a final *R*-factor of 15.5%

17424658, 2005, 10, Downloaded from https://febs.onlinelibrary.wiley.com/doi/10.1111/j.1742-4658.2005.04664.x by University Of Leiden, Wiley Online Library on [17/05/2023]. See the Terms and Conditions (https://onlinelibrary.wiley.com/terms-and-conditions) on Wiley Online Library for rules of use; OA articles are governed by the applicable Creative Commons License

(R_{free} 19.0%). The quality of all models was checked by PROCHECK [33] and WHATIF [61]. The coordinates and structural factors have been deposited in the Protein Data Bank under the accession codes 2bgv, wt, 2bh5, M100K(*rt*) and 2bh4, M100K(cc).

Unfolding monitored by UV/Vis spectroscopy and peroxidase activity

GdmHCl (Aldrich 99%) was dissolved to 8 M in water (Milli-Q) and filtered before use. Solutions ranging from 0 to 6 M GdmHCl were buffered with 100 mM sodium phosphate and the pH of each solution was measured separately. Protein samples were oxidized by addition of 1 mM $K_3[Fe(CN)_6]$ followed by exchange into water by ultra-filtration methods (Amicon). UV/Vis spectroscopy was carried out on a Shimadzu UVPC-2101PC spectrophotometer fitted with a thermostat. Protein concentrations of $\approx$ 5 μM were used. Peroxidase activity was assayed using hydrogen peroxide and guaiacol (*O*-methoxyphenol, Sigma). The synthesis of the fourfold oxidized product of guiacol, 3,3′-dimethoxy-4,4′-biphenoquinone [62] ($\varepsilon_{470} = 26.6\ mM^{-1}cm^{-1}$ [63]) was monitored on the above mentioned spectrophotometer. The resulting activity profiles were analysed as previously described, with the reaction rate depending linearly on $[H_2O_2]$ [12,18]. For coherent graphical representation, the activities are expressed as the biomolecular rate constant of the H_2O_2-cyt *c*-550 reaction. All assays were performed at 298 K with a [guaiacol] of 10 mM, a [cyt *c*-550] between 0.9 and 1.6 μM, and the $[H_2O_2]$ between 0.1 mM and 100 mM.

Unfolding curves were assessed by the two-state model of equilibrium unfolding assuming linear baselines for native and unfolded protein, according to the method of Santoro and Bolen [64]:

$$\text{observable} = \frac{a + b[\text{Gdm.HCl}] + (c + d[\text{Gdm.HCl}])\exp\left(\frac{-\Delta G_{unf} + m[\text{Gdm.HCl}]}{RT}\right)}{1 + \exp\left(\frac{-\Delta G_{unf} + m[\text{Gdm.HCl}]}{RT}\right)} \quad (1)$$

where a and *c* correspond to the values of native and fully unfolded protein at zero denaturant concentration, respectively, and *b* and *d* to their respective dependence on [GdmHCl]. ΔG_{unf} is the Gibbs' free energy of unfolding in the absence of denaturant and *m* represents the dependence of the unfolding free energy on [GdmHCl]. For the fitting of the peroxidase activity data the following modification was applied. Because the native state is assumed fully inactive due to the six coordinate heme-iron being unable to react with H_2O_2 its activity cannot change linearly with increasing [GdmHCl]. Therefore a and *b* (pretransitional baseline) in Eqn (1) were set to zero. The fits (nonlinear least-squares fitting) were generated using the algorithm of Levenberg and Marquardt and performed in the program Origin, version 6.0 (Microcal Software, Northampton, MA, USA).

NMR spectroscopy

Samples to be analysed by NMR contained the desired concentrations of protein (0.5–1.0 mM), GdmHCl (0–4.5 M), 100 mM sodium phosphate and 6% D_2O for lock. The pH of each sample was adjusted to 7.0 by addition of 0.05–1.0 M stock solutions of HCl or NaOH and measured with an NMR pH electrode (Hamilton). All experiments were performed on a Bruker DMX600 spectrometer operating at a ^1H frequency of 600.1 MHz and a temperature of 298 K. 1D ^1H spectra were acquired with presaturation of the residual water signal and a spectral window of 70 p.p.m. Proton T_1 values were measured using an inversion recovery pulse sequence with variable delay times ranging between 0.05 and 0.9 s. All 1D spectra were processed in XWINNMR with exponential multiplication (50 Hz) being applied to each free induction decay before Fourier transformation. Proton T_1 relaxation times were obtained by fitting the peak intensity as a function of the variable delay time to a single-exponential decay in the program Origin.

Acknowledgements

J.A.R.W. and A-M.M.R. are grateful to Dr N.S. Pannu for help with data processing and answers to numerous questions. J.A.R.W. and G.W.C. are grateful to the Netherlands Organization for Scientific Research under the auspices of the 'Softlink' program, grant number 98S1010 for funding. Furthermore we are grateful to the European Synchrotron Radiation Facility at Grenoble, France for provision of synchrotron radiation facilities and we would like to thank Dr P. Carpentier for assistance in using beamline BM30a.

References

1 Katayama Y, Hiraishi A & Kuraishi H (1995) *Paracoccus thiocyanatus* a new species of thiocyanate utilizing facultative chemolithotroph, and transfer of *Thiobacillus versutus* to the genus *Paracoccus* as *Paracoccus versutus* with emendation of the genus. *Microbiology* **141**, 1469–1477.

2 Dennison C, Canters GW, De Vries S, Vijgenboom E & Van Spanning RJ (1998) The methylamine dehydrogenase electron transfer chain. *Adv Inorg Chem* **45**, 351–407.

3 Lommen A, Ratsma A, Bijlsma N, Canters GW, Van Wielink JE, Frank J & Van Beeumen J (1990) Isolation and characterization of cytochrome *c*-550 from the methylamine-oxidizing electron-transport chain of *Thiobacillus versutus*. *Eur J Biochem* **192**, 653–661.

17424658, 2005, 10, Downloaded from https://febs.onlinelibrary.wiley.com/doi/10.1111/j.1742-4658.2005.04864.x by University Of Leiden, Wiley Online Library on [17/05/2023]. See the Terms and Conditions (https://onlinelibrary.wiley.com/terms-and-conditions) on Wiley Online Library for rules of use; OA articles are governed by the applicable Creative Commons License

4 Ubbink M, Van Beeumen J & Canters GW (1992) Cytochrome *c*-550 from *Thiobacillus versutus*: cloning, expression in *Escherichia coli*, and purification of the heterologous holoprotein. *J Bacteriol* **174**, 3707–3714.

5 Ubbink M & Canters GW (1993) Mutagenesis of the conserved lysine-14 of cytochrome *c*-550 from *Thiobacillus versutus* affects the protein structure and the electron self-exchange rate. *Biochemistry* **32**, 13893–13901.

6 Ubbink M, Warmerdam GCM, Campos AP, Teixeira M & Canters GW (1994) The role of lysine-99 of *Thiobacillus versutus* cytochrome *c*-550 in the alkaline transition. *FEBS Letts* **351**, 100–104.

7 Ubbink M, Campos AP, Teixeira M, Hunt NI, Hill HAO & Canters GW (1994) Characterization of mutant Met100Lys of cytochrome *c*-550 from *Thiobacillus versutus* with lysine-histidine heme ligation. *Biochemistry* **33**, 10051–10059.

8 Ubbink M, Hunt NI, Hill HAO & Canters GW (1994) Kinetics of the reduction of wild-type and mutant cytochrome *c*-550 by methylamine dehydrogenase and amicyanin from *Thiobacillus versutus*. *Eur J Biochem* **222**, 561–571.

9 Louro RO, de Waal EC, Ubbink M & Turner DL (2002) Replacement of the methionine axial ligand in cytochrome *c*-550 by a lysine: effects on the haem electronic structure. *FEBS Letts* **510**, 185–188.

10 Ubbink M, Pfuhl M, Van der Oost J, Berg A & Canters GW (1996) NMR assignments and relaxation studies of *Thiobacillus versutus* ferrocytochrome *c*-550 indicate the presence of a highly mobile 13-residues long C-terminal tail. *Prot Sci* **5**, 2494–2505.

11 Worrall JAR, Diederix REM, Prudêncio M, Lowe CE, Ciofi-Baffoni S, Ubbink M & Canters GW (2005) The effects of ligand exchange and mobility on the peroxidase activity of a bacterial cytochrome *c* upon unfolding. *Chembiochem* **6**, 747–758.

12 Diederix REM, Ubbink M & Canters GW (2002) Peroxidase activity as a tool for studying the folding of *c*-type cytochromes. *Biochemistry* **41**, 13067–13077.

13 Diederix REM, Ubbink M & Canters GW (2002) Effect of the protein matrix of cytochrome *c* in suppressing the inherent peroxidase activity of its heme prosthetic group. *Chembiochem* **3**, 110–112.

14 Diederix REM, Busson S, Ubbink M & Canters GW (2004) Increase of the peroxidase activity of cytochrome *c*−550 by the interaction with detergents. *J Mol Catal B: Enzym* **27**, 75–82.

15 Benning MM, Meyer TE & Holden HM (1994) X-ray structure of the cytochrome c_2 isolated from *Paracoccus denitrificans* refined to 1.7 Å resolution. *Arch Biochem Biophys* **310**, 460–466.

16 Sutin N & Yandell JK (1972) Mechanisms of reactions of cytochrome *c*: rate and equilibrium constants for ligand binding to horse heart ferricytochrome. *C J Biol Chem* **247**, 6932–6936.

17 Schejter A & Aviram I (1969) Reaction of cytochrome *c* with imidazole. *Biochemistry* **8**, 149–153.

18 Diederix REM, Ubbink M & Canters GW (2001) The peroxidase activity of cytochrome *c*-550 from *Paracoccus versutus*. *Eur J Biochem* **268**, 4207–4216.

19 Dumortier C, Fitch J, Van Petegem F, Vermulen W, Meyer TE, Van Beeumen JJ & Cusanovich MA (2004) Protein dynamics in the region of the sixth ligand methionine revealed by studies of imidazole binding to *Rhodobacter capsulatus* cytochrome c_2 hinge mutants. *Biochemistry* **43**, 7717–7724.

20 Dumortier C, Fitch J, Meyer TE & Cusanovich MA (2002) Protein dynamics: imidazole and 2-mercaptoethanol binding to the *Rhodobacter capsulatus* cytochrome c_2 mutant, glycine 95 proline. *Arch Biochem Biophys* **405**, 154–162.

21 Dumortier C, Meyer TE & Cusanovich MA (1999) Protein dynamics: imidazole binding to class I *c*-type cytochromes. *Arch Biochem Biophys* **371**, 142–148.

22 Dumortier C, Holt JM, Meyer TE & Cusanovich MA (1998) Imidazole binding to *Rhodobacter capsulatus* cytochrome c_2: effect of site-directed mutants on ligand binding. *J Biol Chem* **273**, 25647–25653.

23 Axelrod HL, Feher G, Allen JP, Chirino AJ, Day MW, Hsu BT & Rees DC (1994) Crystallization and X-ray structure determination of cytochrome c_2 from *Rhodobacter sphaeroides* in three crystal forms. *Acta Crystallogr Sect D: Biol Crystallogr* **50**, 596–602.

24 Geremia S, Garau G, Vaccari L, Sgarra R, Viezzoli MS, Calligaris M & Randaccio L (2002) Cleavage of the iron-methionine bond in *c*-type cytochromes: Crystal structure of oxidized and reduced cytochrome c_2 from *Rhodopseudomonas palustris* and its ammonia complex. *Prot Sci* **11**, 6–17.

25 Assfalg M, Bertini I, Dolfi A, Turano P, Mauk AG, Rosell FI & Gray HB (2003) Structural model for an alkaline form of ferricytochrome. *C J Am Chem Soc* **125**, 2913–2922.

26 Rosell FI, Ferrer JC & Mauk AG (1998) Proton-linked protein conformational switching: definition of the alkaline conformational transition of yeast iso-1-ferricytochrome. *C J Am Chem Soc* **120**, 11234–11245.

27 Hong XL & Dixon DW (1989) NMR study of the alkaline isomerization of ferricytochrome. *C FEBS Letts* **246**, 105–108.

28 Hoang L, Maity H, Krishna MMG, Lin Y & Englander SW (2003) Folding units govern the cytochrome *c* alkaline transition. *J Mol Biol* **331**, 37–43.

29 Englander SW, Sosnick TR, Mayn LC, Shtilerman M, Qi PX & Bai YW (1998) Fast and slow folding in cytochrome. *C Acc Chem Res* **31**, 737–744.

30 Shastry MCR, Sauder JM & Roder H (1998) Kinetic and structural analysis of submillisecond folding events in cytochrome. *C Acc Chem Res* **31**, 717–725.

17424658, 2005, 10, Downloaded from https://febs.onlinelibrary.wiley.com/doi/10.1111/j.1742-4658.2005.04664.x by University Of Leiden, Wiley Online Library on [17/05/2023]. See the Terms and Conditions (https://onlinelibrary.wiley.com/terms-and-conditions) on Wiley Online Library for rules of use; OA articles are governed by the applicable Creative Commons License

31 Yeh SR & Rousseau DL (1999) Ligand exchange during unfolding of cytochrome. *C J Biol Chem* **274**, 17853–17859.
32 Robinson KA, Ladner JE, Tordova M & Gilliland GL (2000) Cryosalts: suppression of ice formation in macromolecular crystallography. *Acta Crystallogr Sect D: Biol Crystallogr* **56**, 996–1001.
33 Pettigrew GW, Gilmour R, Goodhew CF, Hunter DJB, Devreese B, Van Beeumen J, Costa C, Prazeres S, Krippahl L, Palma PN, Moura I & Moura JJG (1998) The surface-charge asymmetry and dimerisation of cytochrome *c*-550 from *Paracoccus denitrificans*: implications for the interaction with cytochrome *c* peroxidase. *Eur J Biochem* **258**, 559–566.
34 Laskowski RA, Macarthur MW, Moss DS & Thornton JM (1993) PROCHECK: a program to check the stereochemical quality of protein structures. *J Appl Crystallogr* **26**, 283–291.
35 Ramakris C & Ramachan GN (1965) Stereochemical criteria for polypeptide and protein chain conformations. 2. allowed conformations for a pair of peptide units. *Biophys J* **5**, 909.
36 Moore GR & Pettigrew GW (1990) *Cytochromes C: Evolutionary, Structural and Physiochemical Aspects*. Springer-Verlag, Berlin.
37 Sevcik J, Lamzin VS, Dauter Z & Wilson KS (2002) Atomic resolution data reveal flexibility in the structure of RNase Sa. *Acta Crystallogr Sect D: Biol Crystallogr* **58**, 1307–1313.
38 Elove GA, Bhuyan AK & Roder H (1994) Kinetic mechanism of cytochrome *c* folding: involvement of the heme and its ligands. *Biochemistry* **33**, 6925–6935.
39 Hammack B, Godbole S & Bowler BE (1998) Cytochrome *c* folding traps are not due solely to histidine-heme ligation: direct demonstration of a role for N-terminal amino group-heme ligation. *J Mol Biol* **275**, 719–724.
40 Russell BS, Melenkivitz R & Bren KL (2000) NMR investigation of ferricytochrome *c* unfolding: detection of an equilibrium unfolding intermediate and residual structure in the denatured state. *Proc Natl Acad Sci USA* **97**, 8312–8317.
41 Shokhirev NV & Walker FA (1998) The effect of axial ligand plane orientation on the contact and pseudocontact shifts of low-spin ferriheme proteins. *J Biol Inorg Chem* **3**, 581–594.
42 Banci L, Bertini I, Bren KL, Gray HB & Turano P (1995) pH-dependent equilibria of yeast Met80Ala-iso-1-cytochrome *c* probed by NMR spectroscopy: a comparison with the wild-type protein. *Chem Biol* **2**, 377–383.
43 Benning MM, Wesenberg G, Caffrey MS, Bartsch RG, Meyer TE, Cusanovich MA, Rayment I & Holden HM (1991) Molecular structure of cytochrome c_2 isolated from *Rhodobacter capsulatus* determined at 2.5 Å resolution. *J Mol Biol* **220**, 673–685.
44 Garau G, Geremia S & Randaccio L (2002) Relationship between hydrogen-bonding network and reduction potential in *c*-type cytochromes. *FEBS Letts* **516**, 285–286.
45 Berghuis AM & Brayer GD (1992) Oxidation state dependent conformational changes in cytochrome. *C J Mol Biol* **223**, 959–976.
46 Langen R, Brayer GD, Berghuis AM, McLendon G, Sherman F & Warshel A (1992) Effect of the Asn52 to Ile mutation on the redox potential of yeast cytochrome *c*: theory and experiment. *J Mol Biol* **224**, 589–600.
47 Mowat CG, Rothery E, Miles CS, McIver L, Doherty MK, Drewette K, Taylor P, Walkinshaw MD, Chapman SK & Reid GA (2004) Octaheme tetrathionate reductase is a respiratory enzyme with novel heme ligation. *Nat Struct Mol Biol* **11**, 1023–1024.
48 Martinez SE, Huang D, Szczepaniak A, Cramer WA & Smith JL (1994) Crystal structure of chloroplast cytochrome *f* reveals a novel cytochrome fold and unexpected heme ligation. *Structure* **2**, 95–105.
49 Buchler JW, Lay KL, Lee YJ & Scheidt WR (1982) A Mononuclear Hydroxoiron (III) complex of a porphinoid ligand system with bifacial steric hindrance. *Angew Chem Int* **21**, 432.
50 Haryono A, Oyaizu K, Yamamoto K, Natori J & Tsuchida E (1998) Electrocatalytic reduction of dioxygen to water by a carbon electrode coated with (eta-oxo)bis[(meso-tetraphenylporphyrinato)iron (III)]: a convenient template for cofacially oriented iron (II) porphyrins. *Chem Lett* **3**, 233–234.
51 Raphael AL & Gray HB (1989) Axial ligand replacement in horse heart cytochrome *c* by semisynthesis. *Proteins: Struct Func Gen* **6**, 338–340.
52 Barker PD & Mauk AG (1992) pH-linked conformational regulation of a metalloprotein oxidation reduction equilibrium: electrochemical analysis of the alkaline form of cytochrome. *C J Am Chem Soc* **114**, 3619–3624.
53 Tezcan FA, Winkler JR & Gray HB (1998) Effects of ligation and folding on reduction potentials of heme proteins. *J Am Chem Soc* **120**, 13383–13388.
54 Enguita FJ, Rodrigues L, Archer M, Sieker L, Rodrigues A, Pohl E, Turner DL, Santos H & Carrondo MA (2003) Crystallization and preliminary X-ray characterization of cytochrome *c′* from the obligate methylotroph *Methylophilus methylotrophus*. *Acta Crystallogr Sect D: Biol Crystallogr* **59**, 580–583.
55 Otwinowski Z & Minor W (1997) Processing of X-ray diffraction data collected in oscillation mode. *Methods Enzymol* **276**, 307–326.

17424658, 2005, 10, Downloaded from https://febs.onlinelibrary.wiley.com/doi/10.1111/j.1742-4658.2005.04864.x by University Of Leiden, Wiley Online Library on [17/05/2023]. See the Terms and Conditions (https://onlinelibrary.wiley.com/terms-and-conditions) on Wiley Online Library for rules of use; OA articles are governed by the applicable Creative Commons License

56 Vagin A & Teplyakov A (1997) MOLREP: an automated program for molecular replacement. *J Appl Crystallogr* **30**, 1022–1025.
57 Bailey S (1994) The CCP4 suite: programs for protein crystallography. *Acta Crystallogr Sect D: Biol Crystallogr* **50**, 760–763.
58 Murshudov GN, Vagin AA & Dodson EJ (1997) Refinement of macromolecular structures by the maximum-likelihood method. *Acta Crystallogr Sect D: Biol Crystallogr* **53**, 240–255.
59 Mcree DE (1999) XtalView Xfit: a versatile program for manipulating atomic coordinates and electron density. *J Struct Biol* **125**, 156–165.
60 Lamzin VS & Wilson KS (1993) Automated Refinement of Protein Models. *Acta Crystallog, Sect D: Biol Crystallogr* **49**, 129–147.
61 Vriend G (1990) What If: a molecular modeling and drug design program. *J Mol Graph* **8**, 52.
62 Doerge DR, Divi RL & Churchwell MI (1997) Identification of the colored guaiacol oxidation product produced by peroxidases. *Anal Biochem* **250**, 10–17.
63 Baldwin DA, Marques HM & Pratt JM (1987) Hemes and hemoproteins. 5. kinetics of the peroxidatic activity of microperoxidase-8: model for the peroxidase enzymes. *J Inorg Biochem* **30**, 203–217.
64 Santoro MM & Bolen DW (1992) A test of the linear extrapolation of unfolding free-energy changes over an extended denaturant concentration range. *Biochemistry* **31**, 4901–4907.

17424658, 2005, 10, Downloaded from https://febs.onlinelibrary.wiley.com/doi/10.1111/j.1742-4658.2005.04664.x by University Of Leiden, Wiley Online Library on [17/05/2023]. See the Terms and Conditions (https://onlinelibrary.wiley.com/terms-and-conditions) on Wiley Online Library for rules of use; OA articles are governed by the applicable Creative Commons License